RSC Applied Interfaces

ROYAL SOCIETY OF CHEMISTRY

PAPER

View Article Online
View Journal | View Issue

Check for updates

Cite this: *RSC Appl. Interfaces*, 2026, 3, 160

Biocompatible ionic liquid-based formulations for topical delivery of ε-poly-L-lysine to combat subcutaneous fungal infections

Muhammad Safaat, [a] Rike Rachmayati, [a] Rie Wakabayashi, [a] Masahiro Goto [ab] and Noriho Kamiya *[ab]

Received 3rd October 2025,
Accepted 1st December 2025

DOI: 10.1039/d5lf00298b

rsc.li/RSCApplInter

The skin is a critical barrier protecting internal organs from external threats, including pathogens, while also regulating body temperature. However, when pathogens invade this barrier, the integrity of the skin can be disturbed, leading to infection and disease. Fungal infections are increasing, as is fungal resistance to existing drugs, posing significant threats to public health. Here, we developed an antifungal polypeptide-based formulation for topical treatment of subcutaneous fungal infections by incorporating ε-poly-L-lysine (EPL), which has antifungal activity, with recently developed ionic liquid-in-oil formulations (IL/Os). Our results indicate that the IL/Os showed efficacy in compromising the integrity of the stratum corneum in a mouse skin model and prevented the electrostatic interaction of EPL with the SC surface. They allow the EPL to penetrate the skin, and prevent it aggregating, thus enabling it to reach the infecting fungus. EPL-loaded IL/Os demonstrated strong activity against *Trichoderma viride* (phylum Ascomycota) growing beneath skin. After storage at 25 °C for 28 days, EPL-loaded IL/Os retained antifungal activity similar to that of freshly prepared samples. These findings highlight the potential of EPL-loaded IL/Os for application in topical antifungal treatments.

Introduction

Fungal infections are a significant global health challenge, with increasing numbers of fungal diseases and cases every year, and increasing resistance to conventional antifungal treatments.[1] Fungal infections pose considerable risks to health because these pathogens target the deeper layers of the skin.[2] Dermatophytes, a group of filamentous fungi, infect keratinized structures, such as skin, hair, and nails, and cause subcutaneous infections. The prevalence of these infections has recently increased rapidly, particularly among immunocompromised individuals.[3] Topical antifungal formulations are commonly used to manage localized infections, offering the advantages of targeted delivery and reduced systemic side effects.

ε-Poly-L-lysine (EPL), a naturally occurring poly-amino acid composed of 25 to 35 L-lysine residues, has reported ability to inhibit a broad range of microorganisms, including fungi. Several mechanisms underlying the antimicrobial effects of EPL have been explored previously.[4,5] The growth of *Candida albicans*, *Fusarium solani*, and *Saccharomyces cerevisiae* has reportedly been inhibited by <100 μg EPL mL^{-1}, although *Aspergillus niger* was not sensitive to EPL at a low concentration.[5–8] It has been approved as a generally recognized as safe (GRAS) substance (no. 000135) by the U.S. Food and Drug Administration and has been used to prolong the shelf life and maintain the quality of various food products, including rice, noodles, beverages, vegetables, and seafood.[9,10] Importantly, upon ingestion, EPL is metabolized into lysine, an essential amino acid, having no known toxicity or adverse effects in humans.[11–13] Because EPL is used widely as a nontoxic food preservative and in the biomedical industry,[14] it is considered a safe alternative to currently used topical antifungal reagents. For example, EPL has been incorporated into the coaxial electrospun polyvinyl alcohol/poly(ε-caprolactone) nanofibers to inhibit the initial growth of bacteria during wound healing.[15] However, the hydrophilic nature of EPL presents challenges for its therapeutic efficacy, because it accumulates in the stratum corneum (SC), the outermost layer of the skin, whereas successful topical formulations require penetration of EPL into deeper skin layers.

In recent years, physical and mechanical enhancement strategies, including microneedle-based delivery, have been developed to improve the transdermal transport of EPL.[16,17] These methods have expanded the potential for delivering not only small-molecule drugs but also macromolecules such as peptides, proteins, and nucleic acids through the skin. However, conventional surfactants and mechanical penetration techniques

[a] *Department of Applied Chemistry, Graduate School of Engineering, Kyushu University, 744 Motooka, Fukuoka 819-0395, Japan.*
E-mail: kamiya.noriho.367@m.kyushu-u.ac.jp
[b] *Division of Biotechnology, Center for Future Chemistry, Kyushu University, 744 Motooka, Fukuoka 819-0395, Japan*

are often associated with transient skin irritation.[18,19] Recently, surface-active ionic liquids (SAILs)[20,21]—particularly those based on choline or amino acid derivatives—have emerged as promising alternatives to traditional surfactants, owing to their tunable physicochemical properties and biocompatibility. Despite their potential, there have been no published reports to date on the *in vitro* topical or transdermal delivery of EPL using ionic liquid systems.

The surface charge of drug carriers plays a critical role in determining their ability to penetrate the skin. Because the SC exhibits an overall negatively charged surface, positively charged EPL tends to interact predominantly with this superficial skin layer, limiting its transdermal delivery. Conversely, negatively charged lipid nanoparticles experience electrostatic repulsion, which restricts their diffusion across the SC.[22]

To overcome these limitations, nanoparticles with near-neutral surface charge have been proposed as candidates for enhancing transdermal delivery, to minimize the electrostatic repulsion with skin barriers.[22] Designing nanoparticle systems that include EPL and have neutral surface charge could improve not only the solubility and stability of the antifungal agent, but also its activity and effectiveness in treating skin infections.

Ionic liquid (IL)-based microemulsions have emerged as promising candidates for enhancing the delivery of active pharmaceutical ingredients. Because of their physicochemical properties, such as high solubility for both hydrophilic and hydrophobic substances, stability in varying conditions, and biocompatibility, IL-based microemulsions are an ideal platform for the encapsulation and controlled release of amphiphilic antifungal agents. Biocompatible and bioactive polymers can be applied in these formulations, aiming to achieve their therapeutic potential. We have recently proposed an antifungal protein-based formulation for the treatment of subcutaneous fungal infections by combining an artificial lipidated chitin-binding domain of an antifungal chitinase (LysM-lipid)[23–25] with a previously developed ionic liquid-in-oil formulation (IL/O) consisting of choline oleate ([Cho][Ole]) as a surfactant, sorbitan monolaurate (Span-20) as a cosurfactant, and choline propionate ([Cho][Pro]) as a nonaqueous polar internal phase in isopropyl myristate (IPM) as a continuous oil phase.[26] The lipid moieties of LysM-lipid and the IL/Os effectively promoted the skin permeation of LysM-lipid.

Here, we investigated the incorporation of EPL into IL/Os (Fig. 1a), aiming to develop a new biocompatible topical antifungal formulation (Fig. 1b). By combining the antifungal potency of EPL with the enhanced delivery capability of IL/Os, this formulation has the potential to overcome the limitations of current topical antifungal treatments.

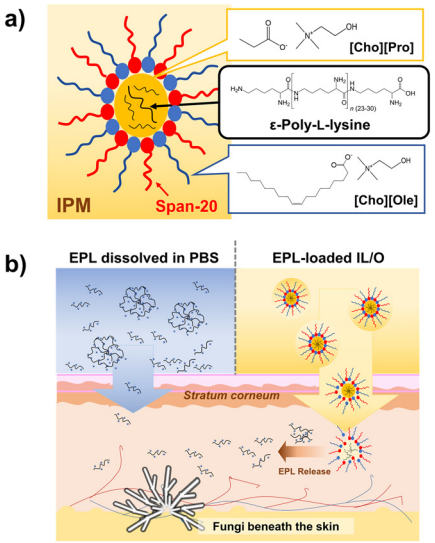

Fig. 1 Treatment of subcutaneous fungal infections with ε-poly-L-lysine (EPL)-loaded ionic liquid-in-oil formulation (IL/O), consisting of choline oleate ([Cho][Ole]) and sorbitan monolaurate (Span-20) in isopropyl myristate (IPM). (a) Schematic illustration showing the structure and components of the IL/O formulation and the possible interaction between EPL and the internal phase choline propionate ([Cho][Pro]). (b) Schematic illustration of the topical delivery of antifungal polypeptide drugs to fungi growing beneath the skin, using phosphate-buffered saline (PBS) and IL/O formulation.

Results and discussion

Preparation and characterization of EPL-loaded IL/O formulations

The effectiveness of topical antifungal treatments depends considerably on their ability to penetrate the SC, facilitating deeper skin absorption. Therefore, enhancing the solubility and permeation of a polymeric antifungal reagent such as EPL is a critical challenge in the development of topical antifungal therapies using EPL. Aiming to address this issue, we incorporated EPL into the core of IL/O formulations by dissolving EPL in [Cho][Pro] and combining this solution with [Cho][Ole] (a surface-active ionic liquid) and Span-20 (a cosurfactant) in IPM to obtain EPL-loaded IL/Os (EPL–IL/Os). We have previously reported that the inclusion of [Cho][Pro] was essential for stabilizing the formulation and enhancing drug encapsulation, while [Cho][Ole], Span-20, and IPM improve the skin permeation.[26,27]

The polydispersity index (PDI) was determined by dynamic light scattering, to assess the particle size distribution of the EPL–IL/Os. The PDI value reflects the uniformity of the particle sizes within a formulation; values below 0.4 indicate a well-defined and homogeneous formulation,[28] while higher PDI values indicate greater heterogeneity. For EPL–IL/O (1 mg mL^{-1}), the measured particle sizes were 256.8 ± 37.6 nm with a PDI of 0.22 (Fig. 2a). In comparison, the hydrodynamic diameter of 1 mg mL^{-1} EPL dissolved in phosphate-buffered saline (PBS) was 507.0 ± 41.9 nm with a PDI of 0.75, indicative of polydisperse formulation. The dynamic light scattering results demonstrated that the IL/O formulations decreased aggregate formation of EPL molecules.

The zeta potential, a measure of surface charge on particles, is a key indicator of the colloidal stability of relevant media.[29–33] The repulsive forces derived from the electrokinetic potential promote particle stability by counteracting attractive van der Waals forces that can cause aggregation. The zeta potential

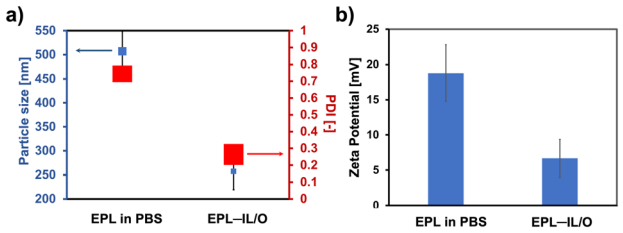

Fig. 2 (a) Particle size and polydispersity index, and (b) zeta potential of EPL in phosphate-buffered saline (PBS) and EPL-loaded IL/O formulations in IPM.

value of the EPL–IL/O in IPM (6.68 mV) was lower than that of EPL in PBS (16.1 mV) (Fig. 2b). In general, colloids with high zeta potentials are electrostatically stable, while those with near-zero zeta potentials are more prone to aggregation because the electrostatic repulsion between particles weakens and the van der Waals attractive forces become dominant.[34] The results thus showed an interesting characteristic of the EPL–IL/O – it has a more uniform formulation than EPL, in which aggregation of EPL is suppressed by the encapsulation in IPM, realizing enhanced overall stability. Meanwhile, the moderate positive surface charge of EPL in PBS (<30 mV) leads to weaker electrostatic repulsion between positively charged EPL chains, which may compromise colloidal stability and promote aggregation.

The performance of a peptide-based formulation largely depends on the stability of the delivery system and its ability to preserve the native structure and biological activity of the peptide. To evaluate the structural integrity of the peptide, we analyzed the secondary structure of EPL after incorporation into the IL and compared it with EPL dissolved in PBS. The circular dichroism (CD) spectra of EPL in IL and PBS are shown (Fig. S1, SI). EPL in PBS exhibited little evidence of conformational structure, consistent with previously reported findings.[35,36] Comparison between freshly prepared EPL in PBS (control) and EPL dissolved in [Cho][Pro]IL as an internal phase revealed no changes in the shape and degree of ellipticity. We further investigated EPL in IL/O formulation. The CD spectrum of EPL–IL/O exhibited a slight increase in negative ellipticity at approximately 217 nm. This shift resembles the spectral change of EPL in alkaline solution, showing a β-sheet formation.[35,36]

Skin permeability study

To effectively deliver drug molecules through the skin, the SC barrier needs to be overcome. Key factors that increase the potential for skin permeability include having a drug molecular weight (MW) of <500 Da, high lipophilicity, and a melting point <200 °C. Because EPL is a hydrophilic, positively charged polymer with MW of approximately 4.1 kDa (Fig. S2, SI), its skin penetration potential is inherently limited. To address this challenge, we prepared EPL-loaded IL/O formulations and investigated the application of these formulations on mouse skin. EPL was chemically conjugated with fluorescein to yield EPL–Flu, enabling the quantification of the EPL content by measuring green fluorescence. Matrix-assisted laser desorption ionization time-of-flight mass spectrometry analysis of EPL–Flu showed a clear shift in m/z values following the conjugation reaction. The observed $\Delta m/z$ (1492 Da) matched well with the theoretical mass increase of chemically modified EPL carrying four fluorescein moieties (1501 Da) (Fig. S2).

The skin permeability of these formulations was evaluated using a Franz diffusion cell (FDC) system with excised mouse skin maintained at 32.5 °C for 6 h. Notably, little EPL penetrated into the skin in PBS, with topical and transdermal permeation amounts of 1.49 and 3.82 μg cm^{-2}, respectively (Fig. 3a). Interestingly, EPL in PBS penetrated across the deeper skin layer markedly higher than that of penetrated within the skin surface. It indicates that once positively charged EPL crosses the stratum corneum, it can easily penetrate deeper into the skin because the underlying layers—viable epidermis and dermis—are hydrophilic and aqueous, allowing a charged, hydrophilic EPL to move more freely. The EPL–IL/O demonstrated 34.2-fold enhanced permeation into the skin compared with EPL in PBS. These results suggest that the IL/O formulation significantly enhanced the permeation of the EPL.

Furthermore, we evaluated the effect of the amount of EPL on the skin permeation of different EPL formulations. Comparative analysis revealed that the transdermal permeation of 100 μg mL^{-1} EPL (in either PBS or EPL–IL/O) was 10-times that of the corresponding 1000 μg mL^{-1} EPL formulation (Fig. 3b). That is, the amount of EPL that permeated transdermally decreased when the initial amount of EPL applied to the skin was increased. Increasing the concentration of a positively charged peptide generally leads to increased aggregation *via* shielding of the negatively charged moieties on peptide chains,[37,38] eventually decreasing the ability of the peptide to be delivered through the skin. Thus, when less EPL is applied to the skin, it is easier for the polycation to adhere to and penetrate the skin's intracellular spaces. We hypothesize that the positive charge and hydrophilic nature of EPL cause it to localize on the negatively charged SC surface, creating a

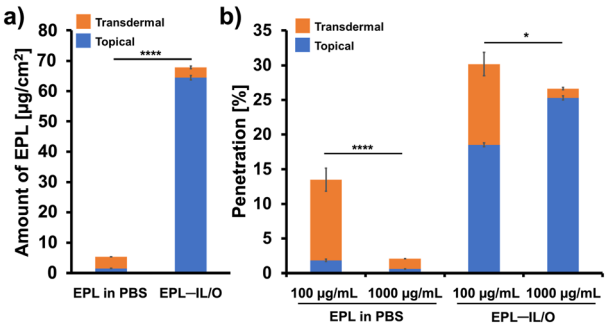

Fig. 3 (a) Skin permeability of EPL in PBS and EPL-loaded IL/Os at 1000 μg mL^{-1} for 6 h. (b) Skin penetration profiles of EPL in PBS and EPL-loaded IL/Os at different initial amounts (1000 and 100 μg mL^{-1}). n = 3, mean ± SD; *P < 0.05 and ****P < 0.0001 indicate that the results were significant compared with 1000 μg mL^{-1} EPL-loaded IL/Os using Tukey's *post hoc* test.

physical barrier to its deeper penetration through the hydrophobic lipids.

Mechanism of skin permeation

The SC intercellular region is organized in a lamellar structure containing various proteins, fatty acids, cholesterol, and ceramides, which together form a strong barrier to drug permeation.[39] This lamellar organization is a key factor affecting drug diffusivity within the intercellular regions. Recently, ILs have gained significant attention as a novel class of permeation enhancers for transdermal drug delivery. It was reported that ILs facilitate drug transport across the skin by modulating both transcellular and paracellular pathways. Their mechanisms of action include disrupting cellular membranes, fluidizing the lipid matrix of the SC, extracting lipid components, and generating new diffusional pathways.[40–43] These effects collectively compromise the integrity of the SC, similar to conventional transdermal enhancers, which typically decrease the barrier function of the skin by altering the tightly packed architecture of corneocytes.[44]

Attenuated total reflection-Fourier transform infrared (ATR-FTIR) spectroscopy is widely used for studying biophysical changes in the SC, particularly in lipid and keratin conformations.[27,45] Here, first, we employed FTIR to evaluate structural changes in the SC lipid alkyl chains after treatment with EPL and EPL–IL/O. The asymmetric CH_2 (ΔV_{as}) stretching vibration (~2918 cm^{-1}) and symmetric CH_2 (ΔV_s) stretching vibration (~2850 cm^{-1}) were used to assess the molecular organization of lipid alkyl chains. The positions of these peaks reflect the structural state of the lipid components, providing valuable information on the internal structure of the lipid bilayer. All treated samples showed some shifts of the absorption peaks to higher wavenumbers. The observed peak shifts indicate an increased ratio of *gauche* to *trans* conformers, reflecting enhanced fluidity of the SC lipids due to disruption of their ordered lamellar structure.[46,47] The magnitudes of the blue shifts in both symmetric (ΔV_s) and asymmetric (ΔV_{as}) CH_2 vibrations were significantly greater for EPL–IL/O-treated samples than for samples treated with EPL dissolved in PBS (Fig. S3a and b). These enhanced spectral shifts suggest that the inclusion of IPM and surface-active ionic liquids in the formulation more effectively perturbed the SC lipid structure, thereby realizing greater enhancement of transdermal permeation.

Among the vibrational spectroscopic features, the amide I (~1630 cm^{-1}) and amide II (~1545 cm^{-1}) bands are particularly informative, because of their sensitivity to alterations in protein secondary structure. These bands thus serve as critical indicators of structural changes within proteins in biological tissues. To assess the effects of EPL-based formulations on the protein conformations within the SC, spectra of the amide region were recorded (Fig. S3c and d). Comparing the changes in the secondary structure of keratin between the two EPL formulations, the EPL–IL/O-treated SC exhibited significantly greater blue shifts in both amide I and amide II vibrational peaks than the SC treated with EPL in PBS (Fig. S3c and d). These blue shifts, corresponding to higher wavenumbers, indicate a structural transition of keratin from an organized α-helix structure to a more disordered, random coil state. Notably, the EPL–IL/O formulation induced a more pronounced reduction in α-helix structure relative to the PBS formulation. It has been shown that disruption of the α-helix structure in keratin contributes to enhanced drug penetration while maintaining a low irritation potential.[48] These conformational changes were attributed to the IL-based formulation, specifically the presence of lipophilic cations, fatty acid-derived anions of the ILs, and IPM, which collectively disrupted the barrier function of the skin.[49] The double-bond carbons of the oleic acid (C18:1) in [Cho][Ole] had a marked effect in facilitating the deformation of the H-bonds in the SC layer compared with the EPL in PBS.[40] Therefore, it can be deduced that preparing EPL–IL/O effectively enhances the skin permeability of EPL.

Antifungal activity

The hydrophilic nature of EPL limits its ability to penetrate the SC, which diminishes its antifungal efficacy when applied topically. To overcome this challenge, we formulated EPL–IL/Os to enhance dermal delivery and facilitate deeper skin penetration, aiming to improve the targeting of subcutaneous fungal infections. To test this idea, we evaluated the antifungal efficacy of EPL in PBS and EPL–IL/Os against *Trichoderma viride*, a model fungal strain of the phylum Ascomycota, growing actively beneath the skin. The antifungal activity assay results are shown in Fig. 4 and S4–S6. Notably, EPL–IL/O exhibited markedly enhanced efficacy, achieving a half-maximal inhibitory concentration (IC_{50}) of approximately 0.1 μg mL^{-1} (Fig. 4a and c and S5). Growth inhibition was observed even at 0.01 μg mL^{-1}, and complete suppression was achieved at 1 μg mL^{-1}. In contrast, EPL in PBS had an IC_{50} value of approximately 10 μg mL^{-1} (Fig. 4b and c and S6), indicating that the IL/O enhanced the antifungal activity of EPL by an order of magnitude. We also tested antifungal activity using water, IPM, and IL/O without EPL, as controls. These controls exhibited negligible inhibition of fungal growth (Fig. S4), confirming that the antifungal activity was derived from the action of EPL.

The enhanced performance of EPL–IL/Os is attributed to the cationic nature of EPL, which interacts with fungal cell membranes, increasing membrane permeability, leading in turn to cytoplasmic leakage and cell lysis.[50–54] Fungal cell death was observed within 12 h of EPL treatment. Interestingly, however, at high concentrations (100–1000 μg mL^{-1}), a paradoxical effect was observed, characterized by the emergence of resistant subpopulations despite the increased EPL exposure. To further investigate this phenomenon, we assessed fungal cell viability and membrane integrity post-EPL treatment (Fig. 4d and S7). EPL exposure led to a marked reduction in viability, with a 78.7% decrease at 1000 μg mL^{-1} after 24 h. These results

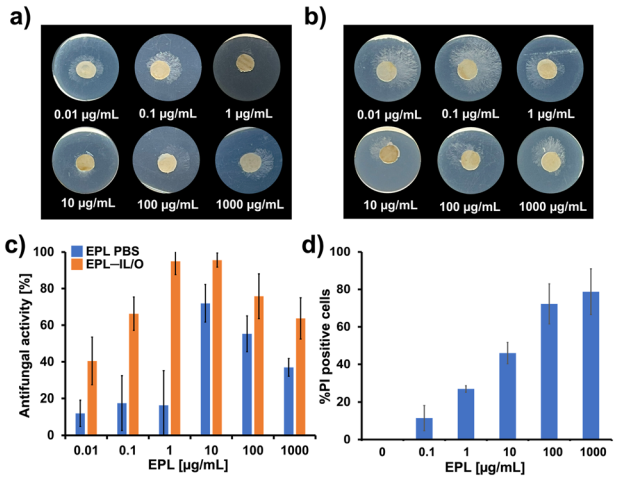

Fig. 4 Topical antifungal activity of EPL-loaded IL/Os. Potato dextrose agar (PDA) plates after subcutaneously growing *Trichoderma viride* were treated topically with (a) EPL-loaded IL/Os and (b) EPL dissolved in PBS at 25 °C for 12 h. (c) Quantitative analysis of the antifungal activity of the EPL-loaded IL/Os and EPL in PBS from the data shown in (a and b). (d) Quantitative analysis of fluorescence microscopy of live/dead *T. viride* cells treated with EPL. As controls, antifungal activity assays were conducted using water, IPM, and IL/O alone (without EPL).

confirm that EPL exerts antifungal effects primarily by compromising membrane integrity without exhibiting the paradoxical effect, supporting its potential as a cationic antifungal agent suitable for topical therapeutic applications.

Stability of EPL-loaded IL/O

IL/Os are generally susceptible to instability during prolonged storage, primarily through the phenomenon of Ostwald ripening.[55] Temperature is a critical factor influencing emulsion stability; elevated temperatures can increase the frequency of particle collisions, promoting aggregation in certain conditions.[56] Here, we assessed the intrinsic physical stability of EPL–IL/Os at 1 mg mL^{-1}, using DLS to determine particle size and PDI. Notably, the particle size of the EPL–IL/Os remained stable over 28 days of storage at 25 °C (Fig. 5). This stability was attributed to the effective interaction between EPL and [Cho][Pro] in the internal phase, which inhibited particle aggregation. In contrast, EPL dissolved in PBS exhibited a gradual increase in particle size over 28 days of storage at 25 °C, with two clearly distributed populations forming by 21 days, one with hydrodynamic diameter in the order of 3–5 nm and the other with hydrodynamic diameter 620–690 nm. The observed PDI for that formulation during storage was >0.4, indicating a lack of uniformity (Fig. 5a and c). These observations suggest that the salt in PBS induced aggregation by shielding the negative charges on peptide chains and serving as salt bridges, which facilitate further aggregation in a long-term storage.

To further investigate the long-term stability and antifungal efficacy of EPL–IL/Os, we conducted topical antifungal assays after 28 day storage at 25 °C. The antifungal activity of EPL was evaluated on the recently developed mouse skin model infected

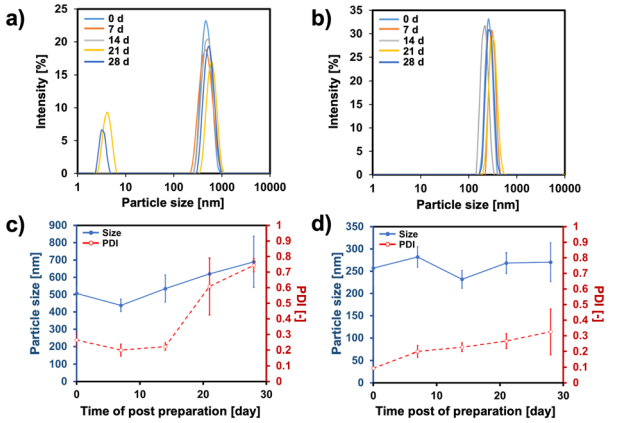

Fig. 5 Physical stability investigated at 25 °C for (a and c) EPL PBS and (b and d) EPL–IL/O, by measuring the changes in particle sizes.

with *T. viride*, and mycelial growth beneath the skin was monitored. Fig. 6 shows topical antifungal activity results after storage of the drug for 28 days at 25 °C. The therapeutic efficacy of the EPL-loaded IL/Os applied topically after storage was comparable to that of freshly prepared EPL–IL/Os (Fig. 6a and S5 and S8). After storage for 28 days at 25 °C, EPL-loaded IL/Os at concentration of 10 μg mL^{-1} was shown to completely suppress fungal growth of *T. viride* within 12 h upon topical application, which is comparable level of antifungal activity with freshly prepared EPL–IL/Os at concentration of 10 μg mL^{-1}. In contrast, after 28 days of storage, EPL in PBS had antifungal activity but at a lower level compared with freshly prepared versions over the tested concentration range of 0.01–1000 μg mL^{-1} (Fig. 6b and S6 and S9). The decreased antifungal activity of EPL in PBS after 28 days of storage could be attributable to aggregation. These results demonstrate that incorporation of EPL with the IL/O inhibits the formation of aggregates of EPL, leading to enhanced stability and sustained antifungal efficacy.

Conclusions

Here, we developed a novel antifungal polycationic peptide formulation based on a recently developed ionic liquid system for the efficient transdermal delivery of EPL. The formulation, incorporated into an ionic liquid-in-oil formulation, was

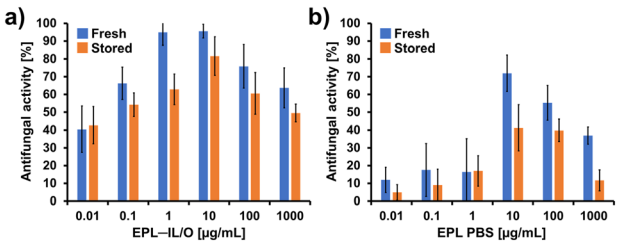

Fig. 6 Quantitative results for the topical antifungal activity of (a) EPL-loaded IL/Os and (b) EPL dissolved in PBS after storage of the drug at 25 °C for 28 days. The photograph of PDA plates with subcutaneously growing *T. viride* treated topically with EPL-loaded IL/Os and EPL in PBS at 25 °C for 12 h are shown in Fig. S8 and S9.

evaluated *in vitro* for its ability to enhance skin penetration and its antifungal efficacy against *T. viride*. The EPL–IL/O formulation had markedly improved transdermal permeation of EPL compared with EPL in PBS, and completely inhibited the growth of *T. viride* beneath mouse skin. This enhanced delivery is likely attributable to a combination of electrostatic interactions between the polycationic EPL and the [Cho][Pro] ionic liquid, which stabilizes the formulation, and the inherent membrane-disruptive properties of the IL components, which may persist as a complex even after penetrating the stratum corneum, leading to effective delivery of EPL through the skin. While EPL served as the model antifungal peptide in this study, the platform is potentially applicable to other polycationic materials and a range of biopharmaceutical agents. In summary, our biocompatible ionic-liquid based formulation is a promising strategy for the effective topical delivery of polypeptide-based antifungal therapeutics.

Experimental

Materials

ε-Poly-L-lysine was purchased from Biosynth (Compton, UK). Propionic acid and choline carbonate were obtained from Wako Pure Chemical Industries Ltd. (Osaka, Japan). Fatty acid (C18:1) and IPM were sourced from Tokyo Chemical Industries Co. Ltd. (Tokyo, Japan). Span-20 was purchased from Sigma-Aldrich (St. Louis, MO, USA). All other reagents and solvents were of analytical grade and used as received without further purification. Mouse skin samples were obtained from Charles River Japan, Inc. (Yokohama, Japan). Amicon Ultra-0.5 centrifugal filters (PLBC Ultracel-3 membrane, 3 kDa) were purchased from Millipore (Tokyo, Japan).

Preparation and characterization of IL/O formulation

The surface-active IL [Cho][Ole] and the nonaqueous polar IL [Cho][Pro] were synthesized according to previously published methods.[20,27,40] The optimal ratios for the IL/O formulations were determined from phase behavior studies of ternary systems. The [Cho][Ole] IL surfactant (7.5 wt%) and cosurfactant (Span-20, 5 wt%) were combined with IPM by vigorous vortexing to achieve a clear homogeneous solution. Subsequently, 2.5 wt% [Cho][Pro], loaded with different concentrations of the polypeptide EPL, was incorporated into the mixture to yield an EPL-loaded IL/O (EPL–IL/O). The size and distribution of the EPL-loaded IL/Os were characterized using dynamic light scattering with a Zetasizer Nano ZS (Malvern Instruments Ltd., UK).

Circular dichroism spectroscopy of EPL in IL

EPL was dissolved in the [Cho][Pro] IL at room temperature, and its secondary structure was subsequently analyzed using circular dichroism (CD) spectroscopy (JASCO, Tokyo, Japan) over the wavelength range of 200–260 nm. To evaluate structural stability, the EPL–IL solution was diluted with PBS (1 : 2 v : v), and 30 μL of EPL–IL in PBS solution at a concentration of 1 mg mL^{-1} was transferred into a quartz cuvette with a 0.1 mm path length for CD measurement. EPL–IL/O formulation was also investigated. Freshly prepared EPL dissolved in PBS served as a control.

In vitro skin permeation study

The transdermal delivery capability of the formulations was evaluated using an FDC system. Fresh mouse skin samples were positioned between the donor and receptor chambers, ensuring that the SC faced upwards. EPL–Flu was prepared by chemically conjugating EPL with 5/6-carboxyfluorescein succinimidyl ester, which was loaded into the prepared IL/O. A 200 μL sample of EPL–Flu-loaded IL/O (100 or 1000 μg mL^{-1}) was applied to the donor compartment, while the receptor phase was filled with PBS (5 mL, pH 7.4), stirred at 500 rpm, and maintained at 32.5 °C. For comparative analysis, EPL–Flu in PBS (1000 and 100 μg mL^{-1}) were also prepared. After 6 h of incubation, the skin was rinsed three times with an extraction solution (PBS : methanol : acetonitrile 2 : 1 : 1 v : v : v) to eliminate residual material. The EPL content in the skin was quantified following established protocols,[26] with skin fragments transferred to microtubes containing 0.5 mL of extraction solution for overnight extraction in the dark. Samples from the receptor chamber were collected for analysis at 6 h. The amount of EPL attached to fluorescein that permeated (transdermal delivery) and remained within the skin (topical delivery) was quantified using a 96-well plate reader with excitation/emission at 494/518 nm.

FTIR study of the SC

FTIR spectroscopy studies on the SC were conducted similarly to the skin permeation assays. SC samples were prepared as circular discs and secured in the FDC with the SC facing upwards. The receptor phase was filled with PBS and maintained at 32.5 °C with continuous stirring. A test solution (0.1 mL, 1 mg mL^{-1}) was added to the donor phase and incubated for 6 h. Post-incubation, the SC samples were washed with 20% ethanol solution and dried at room temperature. A control sample containing only IPM was also prepared in identical conditions. FTIR spectra were obtained using an ATR-FTIR system (PerkinElmer, Waltham, MA, USA), by averaging 20 scans in the range 500–4000 cm^{-1}.

Antifungal activity assay

Topical antifungal efficacy was assessed using a previously reported method.[26] The fungal strain used in this study was from the National Biological Resource Center (NBRC) under accession number NBRC 5702. Briefly, skin pieces (1 cm diameter), which had been loaded with a culture of *T. viride* and had *T. viride* growing actively in the inner layer before use, were placed, hyphae side down, onto a potato-dextrose-agar plate. Test solutions (10 μL) were applied to the outer layer of the skin. The plates were incubated at 25 °C for 12 h and then photographed. The area of fungal growth was subsequently quantified. Antifungal activity, the inhibition percentage (I), was calculated from the equation: $I = [(a - b)/$

$(a - c)] \times 100$ (%), where b is the longest distance of mycelial growth (cm) when treated with EPL-based formulation, a is the longest distance of mycelial growth (cm) when treated with water as a control, assuming that a and b are the diameter of each condition, and c = 1 cm.

Live/dead assay

To evaluate the viability of cells following treatment, cells exposed to the tested formulations were stained with propidium iodide (PI) and 4′,6-diamidino-2-phenylindole (DAPI) as described in the literature.[57] PI is used to stain dead cells (live cells can flush out PI); all cells are stained by DAPI.[58] The fungal cells were prepared according to previously published method.[23] Briefly, *T. viride* spores were inoculated into 10 mL of potato-dextrose broth (PDB) at a final concentration of 10^6 spores per mL and incubated at 25 °C for 18 h with agitation at 150 rpm to promote mycelial growth. The resulting mycelial suspension was centrifuged at 3000 × *g* for 20 min at 25 °C to pellet the mycelia, which were then resuspended in a small volume of fresh PDB. For antifungal activity assays and DAPI/PI staining, samples were prepared across an EPL concentration range of 0.1–1000 μg mL^{-1}. Following treatment, samples were incubated at 25 °C for 1 h, then washed three times with 20 mM sodium phosphate buffer (pH 7.4). Fluorescence imaging was performed using a KEYENCE BZ-800 microscope, and image analysis was carried out using ImageJ software.

Author contributions

M. S.: formal analysis, methodology, investigation, writing the original draft. R. R.: formal analysis, investigation; R. W.: validation, supervision; M. G.: resources, validation, supervision; N. K.: conceptualization, methodology, validation, supervision, writing/reviewing, and editing. All authors contributed to discussion of the paper and approved the final manuscript.

Conflicts of interest

There are no conflicts to declare.

Data availability

All relevant data are within the manuscript and its supplementary information (SI).

Supplementary information is available. See DOI: https://doi.org/10.1039/d5lf00298b.

Acknowledgements

This study was supported by the Japan Society for the Promotion of Science (JSPS) KAKENHI grant number JP23H00247 and AMED under grant number 23ym0126811j0002, Center for Clinical and Translational Research of Kyushu University (to N. K.). M. S. and R. R. express their gratitude to the Japanese Government for awarding a MEXT scholarship. We thank Edanz (https://jp.edanz.com/ac) for editing a draft of this manuscript.

References

1 C. Willyard, *Nature*, 2017, **543**, 15.
2 B. E. Shields, M. Rosenbach, Z. Brown-Joel, A. P. Berger, B. A. Ford and K. A. Wanat, *J. Am. Acad. Dermatol.*, 2019, **80**, 869–880.e5.
3 F. Bongomin, S. Gago, R. O. Oladele and D. W. Denning, *J. Fungi*, 2017, **3**, 57.
4 M. Wei, Y. Ge, C. Li, Y. Chen, W. Wang, B. Duan and X. Li, *Physiol. Mol. Plant Pathol.*, 2018, **103**, 23–27.
5 F. Padilla-Garfias, L. Ríos-Cifuentes, N. S. Sánchez, M. Calahorra and A. Peña, *Biochim. Biophys. Acta, Gen. Subj.*, 2022, **1866**, 130197.
6 T. Yoshida and T. Nagasawa, *Appl. Microbiol. Biotechnol.*, 2003, **62**, 21–26.
7 C. Zhou, P. Li, X. Qi, A. R. M. Sharif, Y. F. Poon, Y. Cao, M. W. Chang, S. S. J. Leong and M. B. Chan-Park, *Biomaterials*, 2011, **32**, 2704–2712.
8 T. Bo, P. P. Han, Q. Z. Su, P. Fu, F. Z. Guo, Z. X. Zheng, Z. L. Tan, C. Zhong and S. R. Jia, *Food Control*, 2016, **61**, 123–134.
9 R. Su, T. Li, D. Fan, J. Huang, J. Zhao, B. Yan, W. Zhou, W. Zhang and H. Zhang, *J. Sci. Food Agric.*, 2019, **99**, 2922–2930.
10 J. Hiraki, T. Ichikawa, S. I. Ninomiya, H. Seki, K. Uohama, H. Seki, S. Kimura, Y. Yanagimoto and J. W. Barnett, *Regul. Toxicol. Pharmacol.*, 2003, **37**, 328–340.
11 Z. Xu, Z. Xu, X. Feng, D. Xu, J. Liang and H. Xu, *Appl. Microbiol. Biotechnol.*, 2016, **100**, 6619–6630.
12 S. C. Shukla, A. Singh, A. K. Pandey and A. Mishra, *Biochem. Eng. J.*, 2012, **65**, 70–81.
13 Y. Q. Li, Q. Han, J. L. Feng, W. L. Tian and H. Z. Mo, *Food Control*, 2014, **43**, 22–27.
14 K. D. Hyde, J. Xu, S. Rapior, R. Jeewon, S. Lumyong, A. G. T. Niego, P. D. Abeywickrama, J. V. S. Aluthmuhandiram, R. S. Brahamanage, S. Brooks, A. Chaiyasen, K. W. T. Chethana, P. Chomnunti, C. Chepkirui, B. Chuankid, N. I. de Silva, M. Doilom, C. Faulds, E. Gentekaki, V. Gopalan, P. Kakumyan, D. Harishchandra, H. Hemachandran, S. Hongsanan, A. Karunarathna, S. C. Karunarathna, S. Khan, J. Kumla, R. S. Jayawardena, J. K. Liu, N. Liu, T. Luangharn, A. P. G. Macabeo, D. S. Marasinghe, D. Meeks, P. E. Mortimer, P. Mueller, S. Nadir, K. N. Nataraja, S. Nontachaiyapoom, M. O'Brien, W. Penkhrue, C. Phukhamsakda, U. S. Ramanan, A. R. Rathnayaka, R. B. Sadaba, B. Sandargo, B. C. Samarakoon, D. S. Tennakoon, R. Siva, W. Sriprom, T. S. Suryanarayanan, K. Sujarit, N. Suwannarach, T. Suwunwong, B. Thongbai, N. Thongklang, D. Wei, S. N. Wijesinghe, J. Winiski, J. Yan, E. Yasanthika and M. Stadler, *Fungal Diversity*, 2019, **97**, 1–136.
15 X. Lan, Y. Liu, Y. Wang, F. Tian, X. Miao, H. Wang and Y. Tang, *Int. J. Pharm.*, 2021, **601**, 120525.
16 R. Luo, D. Xian, F. Li, G. Zhou, L. Jiang, J. Wu and L. Lin, *Int. J. Biol. Macromol.*, 2024, **266**, 131383.
17 D. Xian, R. Luo, Q. Lin, L. Wang, X. Feng and Y. Zheng, *Mater. Today Bio*, 2025, **31**, 101498.
18 C. A. M. Bondi, J. L. Marks, L. B. Wroblewski, H. S. Raatikainen, S. R. Lenox and K. E. Gebhardt, *Environ. Health Insights*, 2015, **9**, 27–32.

19 A. Gowda, B. Healey, H. Ezaldein and M. Merati, *J. Clin. Aesthet. Dermatol.*, 2021, **14**, 45–54.
20 M. K. Ali, R. M. Moshikur, R. Wakabayashi, Y. Tahara, M. Moniruzzaman, N. Kamiya and M. Goto, *J. Colloid Interface Sci.*, 2019, **551**, 72–80.
21 R. Klein, E. Müller, B. Kraus, G. Brunner, B. Estrine, D. Touraud, J. Heilmann, M. Kellermeier and W. Kunz, *RSC Adv.*, 2013, **3**, 23347–23354.
22 A. Tupal, M. Sabzichi, F. Ramezani, M. Kouhsoltani and H. Hamishehkar, *J. Microencapsulation*, 2016, **33**, 372–380.
23 H. Saputra, M. Safaat, K. Uchida, P. Santoso, R. Wakabayashi, M. Goto, T. Taira and N. Kamiya, *RSC Pharm.*, 2024, **1**, 372–378.
24 H. Saputra, M. Safaat, P. Santoso, R. Wakabayashi, M. Goto, T. Taira and N. Kamiya, *Int. J. Mol. Sci.*, 2024, **25**, 3567.
25 M. Safaat, K. Uchida, P. Santoso, R. Sato, T. Taira, R. Wakabayashi, M. Goto and N. Kamiya, *ChemBioChem*, 2025, **26**, e202401081.
26 M. Safaat, H. Saputra, P. Santoso, T. Taira, R. Wakabayashi, M. Goto and N. Kamiya, *ACS Appl. Mater. Interfaces*, 2025, **17**, 3062–3071.
27 M. R. Islam, S. Uddin, M. R. Chowdhury, R. Wakabayashi, M. Moniruzzaman and M. Goto, *ACS Appl. Mater. Interfaces*, 2021, **13**, 42461–42472.
28 A. S. Eissa, *Food Hydrocolloids*, 2019, **87**, 97–100.
29 S. Babita, S. K. Sharma and S. M. Gupta, *Exp. Therm. Fluid Sci.*, 2016, **79**, 202–212.
30 R. Xu, *Particuology*, 2008, **6**, 112–115.
31 Y. B. Yu, C. Wang, T. T. Chen, Z. W. Wang and J. K. Yan, *LWT–Food Sci. Technol.*, 2021, **137**, 110475.
32 S. Al-Anssari, M. Arif, S. Wang, A. Barifcani and S. Iglauer, *J. Colloid Interface Sci.*, 2017, **508**, 222–229.
33 S. U. Ilyas, R. Pendyala and N. Marneni, *Chem. Eng. Technol.*, 2014, **37**, 2011–2021.
34 K. Li, W. Zhong, P. Li, J. Ren, K. Jiang and W. Wu, *Int. J. Biol. Macromol.*, 2023, **252**, 126281.
35 J. Liu, S. Chang, P. Xu, M. Tan, B. Zhao, X. Wang and Q. Zhao, *J. Agric. Food Chem.*, 2020, **68**, 1101–1109.
36 D. R. S. Kushwaha, K. B. Mathur and D. Balasubramanian, *Biopolymers*, 1980, **19**, 219–229.
37 V. N. Vijayan, K. Kannan, R. Sahadevan, A. Jose, M. Porel and S. Sadhukhan, *ACS Appl. Bio Mater.*, 2024, **7**, 4654–4663.
38 M. Seo, K.-J. Lee, B. Seo, J.-H. Lee, J. Lee, D. Shin and J. Park, *Biomolecules*, 2024, **14**, 431.
39 C. M. Beddoes, G. S. Gooris, F. Foglia, D. Ahmadi, D. J. Barlow, M. J. Lawrence, B. Demé and J. A. Bouwstra, *Langmuir*, 2020, **36**, 10270–10278.
40 M. R. Islam, M. R. Chowdhury, R. Wakabayashi, N. Kamiya, M. Moniruzzaman and M. Goto, *Pharmaceutics*, 2020, **12**, 392.
41 C. Agatemor, K. N. Ibsen, E. E. L. Tanner and S. Mitragotri, *Bioeng. Transl. Med.*, 2018, **3**, 7–25.
42 W. Huang, X. Wu, J. Qi, Q. Zhu, W. Wu, Y. Lu and Z. Chen, *Drug Discovery Today*, 2020, **25**, 901–908.
43 L. Zheng, Z. Zhao, Y. Yang, Y. Li and C. Wang, *Int. J. Pharm.*, 2020, **576**, 119031.
44 A. Kováčik, K. Monika and K. Vávrová, *Expert Opin. Drug Delivery*, 2020, **17**, 145–155.
45 M. R. Islam, M. R. Chowdhury, R. Wakabayashi, Y. Tahara, N. Kamiya, M. Moniruzzaman and M. Goto, *Int. J. Pharm.*, 2020, **582**, 119335.
46 S. Kozaka, Y. Tahara, R. Wakabayashi, T. Nakata, T. Ueda, N. Kamiya and M. Goto, *Mol. Pharmaceutics*, 2020, **17**, 645–655.
47 R. Mendelsohn, C. R. Flach and D. J. Moore, *Biochim. Biophys. Acta, Biomembr.*, 2006, **1758**, 923–933.
48 Y. Pyatski, C. R. Flach and R. Mendelsohn, *Biochim. Biophys. Acta, Biomembr.*, 2020, **1862**, 183335.
49 S. N. Pedro, C. S. R. Freire, A. J. D. Silvestre and M. G. Freire, *Int. J. Mol. Sci.*, 2020, **21**, 1–50.
50 C. Liu, H. Liu, C. Wang, F. Kong, H. He and Y. Qiao, *LWT–Food Sci. Technol.*, 2024, **199**, 116057.
51 L. Lin, Y. Gu, C. Li, S. Vittayapadung and H. Cui, *Food Control*, 2018, **91**, 76–84.
52 E. Lebaudy, C. Guilbaud-Chéreau, B. Frisch, N. E. Vrana and P. Lavalle, *Adv. NanoBiomed Res.*, 2023, **3**, 2300080.
53 Z. Tan, Y. Shi, B. Xing, Y. Hou, J. Cui and S. Jia, *Bioresour. Bioprocess.*, 2019, **6**, 11.
54 W. Jiao, X. Liu, Q. Chen, Y. Du, Y. Li, F. Yue, X. Dong and M. Fu, *Postharvest Biol. Technol.*, 2020, **168**, 111270.
55 A. Chebil, J. Desbrières, C. Nouvel, J. L. Six and A. Durand, *Colloids Surf., A*, 2013, **425**, 24–30.
56 A. Hosseini, S. M. Jafari, H. Mirzaei, A. Asghari and S. Akhavan, *Carbohydr. Polym.*, 2015, **126**, 1–8.
57 A. Stringaro, M. Colone, S. Cecchetti, E. Zeppetella, F. Spadaro and L. Angiolella, *Arch. Microbiol.*, 2023, **205**, 15.
58 Z. Darzynkiewicz, X. Li and J. Gong, *Methods Cell Biol.*, 1994, **41**, 15–38.